eng

Article

Enhancing Wear Resistance of Drilling Motor Components: A Tribological and Materials Application Study

Achouak Benarbia [1], Olusegun Stanley Tomomewo [1,*], Aimen Laalam [2,*], Houdaifa Khalifa [1], Sarra Bertal [3] and Kamel Abadli [3]

[1] College of Engineering and Mines Energy Studies, University of North Dakota, Grand Forks, ND 58202, USA; achouak.benarbia@und.edu (A.B.); houdaifa.khalifa@und.edu (H.K.)
[2] Petroleum Engineering Department, University of North Dakota, Grand Forks, ND 58202, USA
[3] Materials Engineering Department, National Polytechnic School, El Harrach, Algiers 16200, Algeria; sarra.bertal@g.enp.edu.dz (S.B.); kamel.abadli@g.enp.edu.dz (K.A.)
* Correspondence: olusegun.tomomewo@und.edu (O.S.T.); aimen.laalam@und.edu (A.L.)

Abstract: The oil and gas industry faces significant challenges due to wear on drilling motor components, such as thrust pins and inserts. These components are critical to the efficiency and reliability of drilling operations, yet are susceptible to wear, leading to significant economic losses, operational downtime, and safety risks. Despite previous research on wear-resistant materials and surface treatments, gaps exist in understanding the unique properties of thrust pins and inserts. The aim of this study is to enhance mechanical system performance by characterizing the wear resistance of these components. Through chemical analysis, hardness assessments, and metallographic examinations, the study seeks to identify specific alloys and microstructures conducive to wear resistance. Key findings reveal that AISI 9314 thrust pins exhibit superior wear resistance with a tempered martensite microstructure and a hardness of 41 HRc, whereas AISI 9310 inserts are less resistant, with a hardness of 35 HRc. The research employs advanced techniques, including a pin-on-disc tribometer, scanning electron microscopy (SEM), energy-dispersive X-ray spectroscopy (EDS), and profilometry, to evaluate wear behavior, visualize wear patterns, analyze elemental composition, and quantify material loss and surface roughness. Our findings demonstrate that optimizing the material selection can significantly enhance the durability and efficiency of drilling motors. This has profound implications for the oil and gas industry, offering pathways to reduce maintenance costs, improve operational efficiency, and contribute to environmental sustainability by optimizing energy consumption and minimizing the carbon footprint of drilling operations.

Keywords: thrust pin and insert; wear resistance; tribology; characterization; drilling motors

Citation: Benarbia, A.; Tomomewo, O.S.; Laalam, A.; Khalifa, H.; Bertal, S.; Abadli, K. Enhancing Wear Resistance of Drilling Motor Components: A Tribological and Materials Application Study. *Eng* **2024**, *5*, 566–588. https://doi.org/10.3390/eng5020032

Academic Editors: Zhengyi Jiang and Antonio Gil Bravo

Received: 9 January 2024
Revised: 17 March 2024
Accepted: 5 April 2024
Published: 8 April 2024

1. Introduction

Wear resistance is a paramount consideration in the selection of materials for industrial applications, especially in sectors like the oil and gas industry, where the economic and technical implications of wear can be profound [1]. This encompasses not only increased maintenance costs, but also potential operational inefficiencies. Addressing these challenges necessitates a deep understanding of the materials in use, and materials engineers are at the forefront of this endeavor, aiming to optimize the life cycle and performance of these materials [2].

The oil and gas industry involves intricate drilling operations using mechanical rigs that penetrate the earth's subsoil to perform tasks such as acquisition, development, and production of oil and gas [3]. This process involves employing various parameters, equipment, and tools, like torque and drag software, which assist in selecting drill pipes capable of withstanding torque and drag forces [4]. An essential element of this operation is the drill motor, commonly known as a mud motor. It amplifies the drill bit's power using drilling fluid, and its efficiency is especially paramount in complicated well trajectories, frequently found in aggressive environments [5].

In countries like Algeria, where formations are particularly demanding, drilling often resorts to specialized high-speed (HS) motors. These motors, while presenting opportunities for enhanced drilling and increased penetration rates, also face challenges such as wear, temperature sensitivity, and power constraints [6,7]. High-speed drilling is a vital part of the oil and gas industry, but it puts critical components like thrust pins and inserts, which are essential components of the mud motor's transmission section (Figure 1), under extreme mechanical stress and wear [8]. While numerous studies have investigated the general wear mechanisms in drilling operations, there remains a limited understanding of the wear behavior specific to thrust pins and inserts, (Figure 2), in high-speed drilling motors. Given their critical role in the drilling process, a focused analysis on these components is essential to enhance the efficiency and longevity of drilling operations.

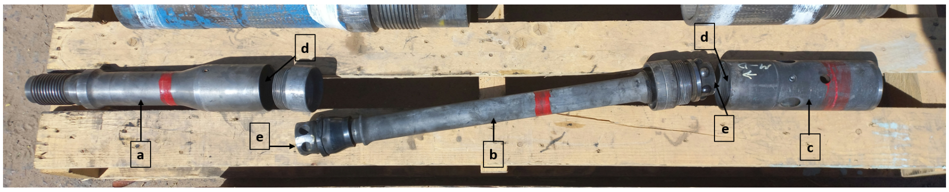

Figure 1. Transmission section parts representing (**a**): rotor coupling, (**b**): transmission shaft, (**c**): shaft coupling, (**d**): location of the insert inside the couplings, and (**e**): location of the pin in the two ends of the transmission shaft.

Figure 2. New thrust pin and insert compared to damaged ones, where (**a**) is the thrust pin and (**b**) the thrust insert.

The thrust pin typically crafted from hardened steel, transmits axial loads and counters abrasive forces during drilling, which can stem from weight on the bit, torque, or drilling forces [9]. Partnering the thrust pin is the thrust insert, generally composed of low-friction or self-lubricating materials, ensuring the efficient transfer of these axial loads [10]. These components act as sacrificial barriers, protecting the transmission shaft from shocks and intense forces. When the thrust pin gets damaged, it can develop a protrusion or deformation. As a result, when the damaged pin comes into contact with the insert, it creates impact marks on the thrust insert. The continuous shocks and impacts can lead to the formation of visible indentations or prints on the insert's surface (Figure 2). Such failures can severely hamper the motor's function, which might mean that some parts of the motor get damaged or broken, making it hard for the motor to keep working properly leading to Pull Out of Hole (POOH) operations to replace the damaged components and restore motor efficiency.

This kind of operation can be expensive because it takes time and requires special tools and skills [11].

Furthermore, these failures can also result in prolonged downtime, which can have a significant impact on the overall productivity of the drilling operation. Additionally, investing in high-quality components and equipment not only enhances the efficiency of the drilling operation, but also prolongs the life of the motor and its components. By taking a proactive approach towards motor maintenance, operators can minimize downtime and maximize efficiency, ultimately leading to increased profitability for their operations [12].

Understanding the wear behavior of drilling components is of utmost importance. The mechanisms of wear in drilling operations are intricate, influenced by numerous factors [13]. This research is pivotal in optimizing energy systems by honing the efficiency of drilling motors, specifically through the in-depth analysis of the wear resistance of thrust pins and inserts—central components of the motor. By understanding the details of how wear happens and introducing stronger materials, there is a focused attempt to reduce stops in drilling activities that would help in reducing upstream losses. This not only translates to remarkable time and energy savings but, crucially, it plays a significant role in reducing CO_2 emissions, making it a cornerstone for a more sustainable energy system.

Highlighting the substantial global energy usage attributed to friction and wear within the mining sector underscores the potential for substantial energy consumption reduction by optimizing wear resistance. This, in turn, could yield a significant decrease in CO_2 emissions, exerting a direct influence on the environmental impact of mining. Holmberg et al. (2017) [14] conducted calculations revealing that friction and wear are responsible for an annual release of 970 million tonnes of CO_2 emissions on a global scale within the mineral mining sector, constituting 2.7% of the world's total CO_2 emissions. In research sourced from a study by Holmberg and Erdemir (2019) [15] on the global impact of tribology on energy use and CO_2 emissions, the study of friction and wear offers significant potential savings. In the short term (5–10 years), it is estimated that we could save EUR 174,000 million and reduce 290 million tonnes of CO_2 emissions. In the long term (15–25 years), the savings could escalate to EUR 576,000 million and a reduction of 960 million tonnes of CO_2 emissions. This can be achieved through technological advancements including nanotechnology, biomimetics, and integrated computational material engineering.

This paper consists of four main sections that explore various aspects of the topic. First, we introduce the critical role of wear resistance in the oil and gas industry, emphasizing the damage to thrust pins and inserts in high-speed drilling motors and their impact on efficiency and downtime. This sets the stage for a focused analysis to enhance the longevity of drilling operations and reduce CO_2 emissions.

Next, we present the experimental work conducted in our research, which included characterizing samples, conducting wear testing, and analyzing damage. Finally, we analyzed the wear characteristics of different steel grades and evaluated their performance.

The paper concludes by weaving together a summary of the findings and their implications for optimizing thrust pins and inserts in high-speed drilling motors. We also provide perspectives for future research directions and potential avenues for further improving wear resistance in drilling components.

2. Literature Review

Components in the oil and gas industry can experience harsh operating environments, which can shorten their lifespan. Wheeler (2018) [16] reported that the degradation processes can be caused by abrasion, erosion, corrosion, or a combination of these factors. Abrasion can occur during drilling operations, while the erosion of valves and pipelines can be caused by sand particles in hydrocarbon fluid flows.

The operating conditions for drilling motor components can be extremely challenging, with high dynamic loads and vibrations. Sexton and Cooley (2009) [17] described some alternatives to diamond thrust bearings, such as rolling-element (ball) bearings and tapered roller bearings. However, ball bearings are susceptible to erosion, while tapered roller bearings need to be sealed from the drilling fluid and require pressure compensation for the bearing assembly.

Tribology is a multidisciplinary field that integrates knowledge from various domains. It centers on examining the interactions that arise when two entities make contact and move relative to each other. This empowers tribologists to investigate and forecast aspects like friction, lubrication, wear, and other related tribological events [18]. In this research, a device known as a tribometer, or tribotester, was employed to mimic and analyze the friction and wear between different surfaces. Dzaky et al. (2021) [19] emphasized the significance of this testing method in the field of tribology as it provides researchers and engineers with a tool to study how materials react, delve into the intricacies of friction and wear, and assess the efficiency of various surface treatments and protective coatings.

Tribometers allow for the meticulous adjustment of test variables like load, speed, and temperature, which ensures consistent results and aids in making comparisons. This instrument uses specimens that come into contact and slide against each other, generating frictional forces (Figure 3). These data aid in defining the tribological attributes of materials, evaluating their behavior under various conditions, and directing the formulation and enhancement of surfaces and lubrication mechanisms, as highlighted by Böttcher et al. (2018) [20]. There are various kinds of tribometers, including pin-on-disk, ball-on-disk, and reciprocating variants. Among these, pin-on-disk tribometers are especially common in tribological studies. This type of tribometer consists of a fixed pin and a spinning disk, facilitating systematic experiments and the assessment of materials and lubricating substances, as noted by Ahmer et al. (2019) [21].

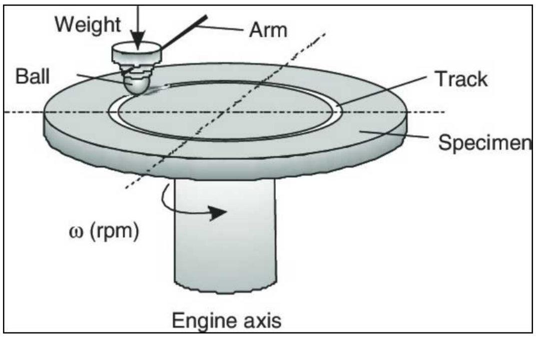

Figure 3. Schematic illustration of pin-on-disc tribometer [22].

Wear analysis and characterization have been the focus of numerous studies over the years, striving to understand and improve the wear resistance of various materials. The following research works provide significant insights into this crucial area of study.

Bill (1978) [23] explored the fretting wear of uncoated AISI 9310 steel and its interaction with various surface coatings. The study utilized wear measurements and SEM observations to identify the primary wear mechanism for uncoated 9310 steel as surface spallation caused by localized fatigue. Notably, the research highlighted the significant impact of environmental humidity on increasing fretting wear and altering debris characteristics. Among the tested coatings, aluminum bronze with polyester and chromium plate were particularly effective in mitigating wear, with the former providing a self-lubricating film and the latter offering robust protection against fretting. This study presents a thorough examination of fretting mechanisms and coating efficacy, yet it suggests further exploration into the long-term effects of different environmental conditions and the durability of coatings under varied operational scenarios.

Building on the understanding of surface treatments, Hartley and Hirvonen (1983) [24] conducted an in-depth analysis of the friction and wear behavior of AISI 9310, 3135, 52100 steels under high load conditions, aiming to understand and mitigate sudden severe adhesive wear. Employing a Falex friction and wear tester, the study examined the effects of various ion implantations and ion beam mixed steels at loads sufficient to induce scuffing.

With a focus on AISI 9310 steel, significant findings included the effective reduction of wear and friction through Ta+ and Mo+ implantations, especially under lower load conditions. The study's innovative approach to using ion implantation for wear resistance provides valuable insights into enhancing steel performance under extreme conditions. However, the research also notes the necessity for further investigations into a broader range of implanted elements and the role of oxides in scuffing prevention.

Yan et al. (2023) [25] further expanded the understanding of AISI 9310's wear characteristics by conducting an extensive investigation into rolling-sliding contact fatigue (RSCF) failures. Utilizing a twin rollers fatigue test rig, the study assessed fatigue life, microstructural evolutions, and residual stress variations under increasing Hertzian contact pressures. Notably, the research demonstrated that shot peening post-carburizing significantly improved RSCF life and microhardness due to enhanced compressive residual stress and a reduction in retained austenite. The study also reported a first-time observation of several ideal shear texture components of body-centered cubic materials due to RSCF. Despite its comprehensive analysis, the study suggests further exploration into the long-term effects of different surface treatment combinations and their practical implications in operational environments.

In the context of high-temperature tribological behavior, Ganechari et al. (2011) [26] focused on AISI 9310, among other steels. The study performed dry sliding wear tests under various temperatures, speeds, and pressures to understand the changes in surface roughness and hardness. For AISI 9310, the findings highlighted that hardness decreased with increasing temperature, while the highest roughness was observed at room temperature. This study provides valuable insights into the wear behavior of AISI 9310 steel under high-temperature conditions, pointing to the necessity for further research on the material's performance over longer periods and under more varied environmental conditions.

A recent study by Li et al. (2022b) [27] on the wear resistance of AISI 9310 steel using Micro-Laser Shock Peening (Micro-LSP), a novel surface modification technique, investigated the effects of different pulse energies on surface morphology, mechanical properties, and wear behavior. It was found that Micro-LSP significantly enhanced surface roughness, increased microhardness, and reduced the coefficient of friction, thereby improving wear resistance by 50% to 70%. The research presents a promising approach to enhancing the wear resistance of AISI 9310 steel; however, it also indicates the need for more detailed studies on the long-term durability of Micro-LSP-treated surfaces under various operational conditions and on a larger scale.

In another aspect of tribology studies, Hegadekatte et al. (2008) [28] worked on a simplistic numerical tool that can be used to identify the wear coefficient from pin-on-disc experimental data and also predict the wear depths within a limited range of parameter variation. Suresh et al. (2017) [29] used simulation and experimental analysis to investigate the tribological characteristics of wear for various loading conditions of an aluminum Metal Matrix Composite (MMC) pin-on-disc tribometer, and found that the simulation results were in line with the experimental results.

In this paper, we delve into the critical issue of wear resistance in the oil and gas industry, with a specific focus on the high-speed drilling operations that are central to the exploration and extraction processes. Our goals are to provide a comprehensive understanding of the wear behavior of thrust pins and inserts in drilling motors, components that are crucial for maintaining the efficiency and longevity of drilling operations, especially in demanding environments like those found in Algeria. Through a detailed analysis, we aim to identify the factors contributing to wear and assess the performance of different materials under operational stresses. Our research contributions are twofold: first, we enhance the current understanding of wear mechanisms in high-speed drilling motors, thereby addressing a significant knowledge gap. Second, by exploring the potential for using advanced materials to improve wear resistance, we offer practical insights that can lead to improved operational efficiency, reduced downtime, decreased energy consumption, and, ultimately, a reduction in CO_2 emissions.

3. Experimental Work

The method used in this study involves a comprehensive chemical analysis to determine the material composition, which is crucial for understanding the foundational properties of the components. This initial step is vital, not only for identifying the steel grade, but also for ensuring the methodology's applicability to materials with similar compositions in various contexts. Following this, the method includes an assessment of microstructural characteristics and hardness properties that would influence wear resistance.

The evaluation of wear resistance is centered around the use of a pin-on-disk tribometer, a choice that highlights the methodology's adaptability to simulate a wide range of wear mechanisms under controlled conditions. This instrument's versatility is complemented by detailed analyses using scanning electron microscopy (SEM) and profilometry techniques to allow an in-depth examination of wear patterns and degradation at both micro- and nanoscales. These combined analytical approaches form a robust and comprehensive framework for investigating wear resistance of any mechanical component in various industrial operations, far beyond the specific case of high-speed drilling motors.

3.1. Chemical Analysis

The thrust pin and insert were sectioned using an electro-erosion machine, making sure to get a sufficient flat surface for conducting the chemical analysis. The samples were then cleaned and subjected to an Optical Emission Spectroscopy (OES) with a SPECTRO MAXx machine (AMETEK SAS Division, Elancourt, France) (Figure 4). To identify their steel grade, following the ASTM E415 standard [30], they were positioned in an appropriate sample holder to ensure optimal contact with the device, allowing for precise spectral data collection over an adequate duration. This analysis was repeated three times for each specimen to guarantee consistency and statistical relevance. The derived results were then juxtaposed with standard materials to confirm the steel grade.

Figure 4. Optical Emission Spectrometer for conducting chemical analysis.

3.2. Microstructural Analysis

Samples were polished using silicon carbide (SiC) abrasive discs beginning with P120 and advancing to P2400, in addition to being further refined using alumina suspension on a felt paper. This step aimed to achieve a mirror-like finish on the sample surfaces, enhancing their reflectivity and facilitating accurate microscopic observation. After that, the polished samples were etched with 4% Nital for 12 s and utilizing a NIKON optical microscope (Ile-de-France, France), which has a maximum resolution of about 200 nm (Figure 5), at magnifications of 1000× and 1500×; the material was inspected at different depths in accordance with ASTM E407 standard [31], offering an understanding of the microstructural characteristics.

Figure 5. Optical microscope used to reveal the microstructure of the samples.

3.3. Hardness Testing

The primary objective of testing both the thrust pin and insert was to ascertain their mechanical attributes, including strength, wear resistance, toughness, and longevity. The samples underwent the Rockwell hardness test using a MITUTOYO machine (Kanagawa, Japan) (Figure 6), which employs a diamond cone indenter to make a mark on the test material according to the ASTM E18 standard [32]. The Rockwell hardness value is noted once the gauge settles, indicating the depth difference between the starting zero point and the ultimate indentation depth.

Figure 6. Rockwell hardness measurements machine.

Then, the steel samples were characterized using a Nikon 600 Vickers microhardness machine (Ile-de-France, France), as shown in (Figure 7). This process aimed to pinpoint differences in hardness throughout distinct sections of the steel specimen following the ASTM E384 standard [33]. By comparing these results with the identified microstructure, connections between the steel's characteristics and its microstructural details were drawn. Additionally, this analysis helped determine whether any surface treatments had been previously applied.

Figure 7. Vickers microhardness measurements machine.

3.4. Tribometer

The Universal and Versatile Ball-Disc and Linear Oscillating Tribometer (Tribo Technic, Paris, France) (Figure 8) was utilized for the rotational disc, and was operated in accordance with the ISO 7148-1 standard [34]. It offers ultra-precise measurement of wear rate in the range of micrometers. The pin or the insert samples were placed in the holder for testing, ensuring both wereanalyzed under identical conditions. The ball used had a 5.5 mm diameter, a martensitic microstructure, and a hardness ranging from 60 to 66 HRc, constructed from AISI 52100. It was imperative for us that the laboratory test replicated real-world conditions as closely as possible. The following parameters were meticulously chosen according to the drilling operation and were input into the machine's software:

- Speed: 110 mm/s.
- Duration per load: 30 min.
- Wear groove: 3 mm.
- Load variations: 4 N, 6 N, 8 N, 10 N, and 12 N.
- Sliding length: 200 m.
- Environmental temperature: 23 °C.

Figure 8. Ball-on-disk tribometer used for analyzing wear resistance of the trust pin and insert.

We first started by applying a range of loads that varied from 4 N to 12 N, which is the maximum load that can be applied using that tribometer. After that, we placed the specimens in the holder that turns with a speed of 110 mm/s specifically chosen according to the rotational speed used during the drilling operation, which was 30 RPM. The last parameter we fixed was the sliding distance of 200 m in a way that makes it close to the drilled depth (185 m). Fixing the speed and distance resulted in a duration of 30 min per load applied.

3.5. Profilometer

The same tribometer was used, equipped with a profilometer installation capable of measuring the worn surface of the track with high accuracy. The profilometer had a resolution of 7.55 nm in the Z-axis and was equipped with a skidless tracer with an internal reference (Figure 9). This allows precise measurements to be taken on samples as small as 2 mm. In contrast, a tracer with a skid requires samples of at least 35 mm in size. It was employed to evaluate the depth of the wear groove, assessing the degree of wear and the quantity of material lost. This instrument produces a chart depicting the wear depth and the region of the wear track section. For more accurate results, we repeated all the measurements at multiple locations within the wear region and calculated an average wear depth and section. The software then utilizes these measurements to compute the wear coefficient. It is given by

$$K_w = \frac{S 2\pi R}{F_n 2\pi n} \quad (1)$$

where:

- K_w: wear coefficient ($mm^3/N.m$).
- S: track section (mm^2).
- n: number of rounds.
- R: radius track (mm).
- F_n: normal load on friction surface (N).

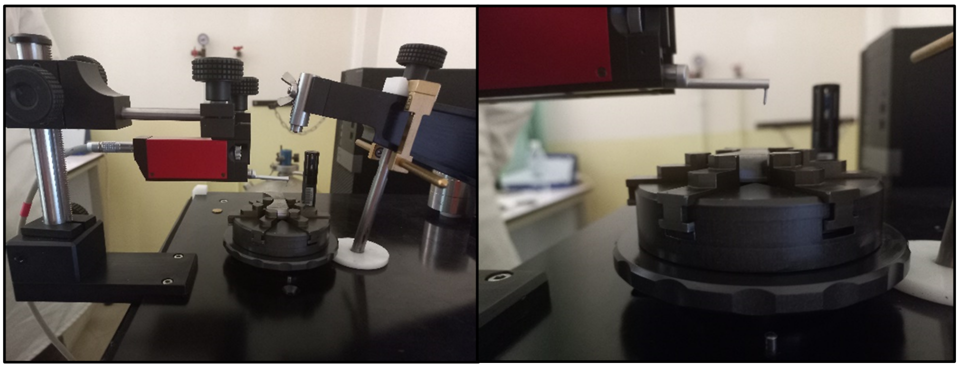

Figure 9. Stylus-type profilometer.

3.6. Scanning Electron Microscopy SEM

The FEI Quanta 650 FEG scanning electron microscope (Thermo Fisher Scientific, Waltham, MA, USA)has a resolution reaching the sub-nanometer level, a magnification range from 5× to an impressive 1,000,000×, and is equipped with several detectors, including secondary electron (SE) and backscattered electron (BSE) detectors (Figure 10). The primary objective of using it consists of the two following aspects:

- Surface examination: the steel samples' surfaces are meticulously inspected for any imperfections, fractures, or applied surface treatments. Energy Dispersive X-ray Spectroscopy (EDS) is utilized to determine their elemental composition.
- Wear mechanism identification: by offering magnified views of wear patterns, scratches, cracks, and other surface damages from the tribology test, SEM aids in pinpointing wear mechanisms, including adhesive, abrasive, or fatigue wear. This is vital for understanding wear causes and devising apt solutions.

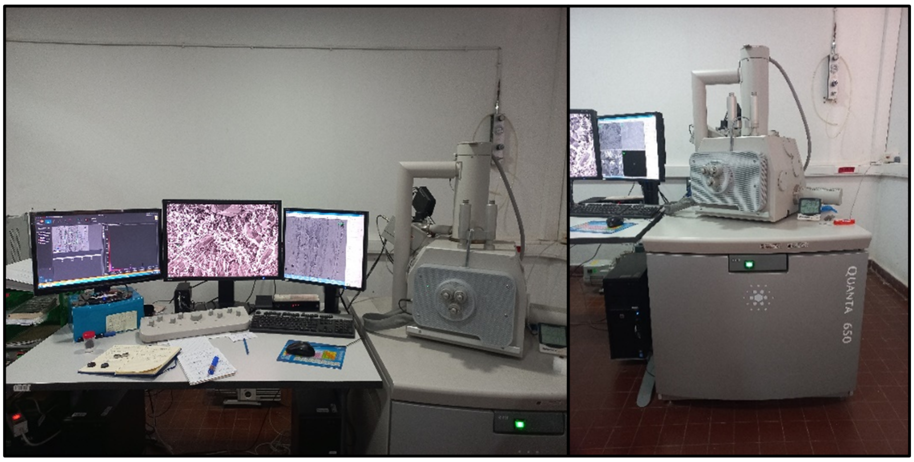

Figure 10. Scanning electron microscope.

Following the ASTM E1508 standard [35], the steel specimen, once prepared, was fixed to SEM stubs with the aid of carbon tape and subsequently placed inside the SEM chamber. The SEM settings employed were 15 KV acceleration voltage, with the working distance and spot size adjusted according to the specimen and the desired imaging resolution. To obtain a detailed view of the steel sample's surface morphology, either secondary electron imaging (SEI) or backscattered electron imaging (BEI) was used.

Concerning the EDS analysis, the SEM was equipped with an EDS detector, which allowed for the elemental analysis following the acquisition of SEM images of the steel surface. This approach relies on the interaction between X-rays and the sample to identify and measure the elements present on the surface, as well as to assess the elemental distribution within the wear groove.

4. Results and Discussion

4.1. Surface Treatment Characterization

The aim of this section of the study was to examine if any surface modifications had been implemented on the trust pin and to validate the claims made by industry engineers regarding the components' origins. This assessment involved a combination of microhardness testing and scanning electron microscopy (SEM) analysis paired with Energy-Dispersive X-ray Spectroscopy (EDS) to detect and analyze the surface treatment being applied.

4.1.1. Microhardness Measurements

The illustrated steel hardness profile in Figure 11 demonstrates how the depth of a coating can be determined from the surface by conducting a series of hardness measurements perpendicular to the surface of the component. The results revealed interesting patterns in the distribution of hardness within the samples tested (Figure 2). Specifically, there was a sharp drop in hardness at a depth of 1.35 mm below the surface, followed by a gradual decrease towards the core. This suggests that the hardening process used in the production of this steel creates a distinct layer of hardened material near the surface, which gradually tapers off towards the interior. It would be interesting to investigate how variations in the hardening process affect this layer and whether it has any impact on other mechanical properties of the steel.

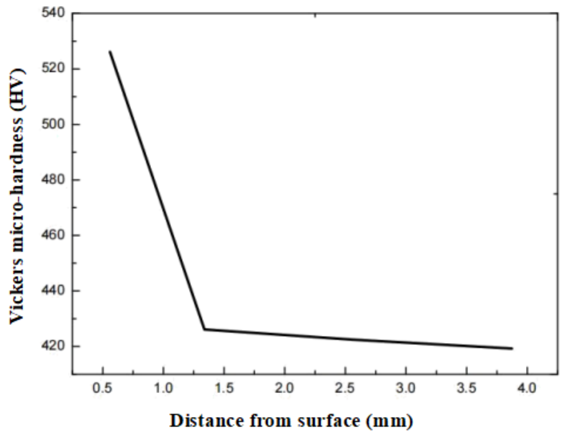

Figure 11. Microhardness profile.

4.1.2. SEM Surface Treatment Characterization

This part of the study is centered on examining the surface characteristics of thrust pins and inserts that may have undergone particular surface treatments. The aim is to understand the chemical composition and microstructure in proximity to the surfaces and establish connections between these outcomes and the results derived from microhardness testing. Differences in hardness between the surface and inner regions imply potential localized surface treatments. To support these observations, surface analysis is conducted using scanning electron microscopy (SEM) coupled with Energy Dispersive X-ray Spectroscopy (EDS) analysis.

The combination of SEM and EDS analyses offers a thorough understanding of the surface chemistry by detecting and quantifying the material's elemental composition. Thess data aid in identifying chemical alterations stemming from surface treatments. Regarding the micrographs showcased in Figure 12, there is no apparent distinction between the microstructures of the area with a hardness value of 526.13HV and the one with 426.12 HV. Both of them exhibit a martensitic structure, with the only noticeable difference being the presence of pores in various sections of the specimen.

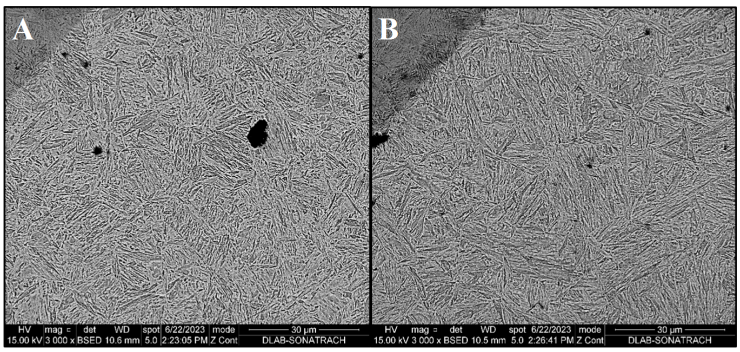

Figure 12. SEM micrographs of (**A**) microstructure near indentation of 526.13 HV and (**B**) microstructure near indentation of 426.12 HV, at a magnification of 3000×.

An Energy Dispersive X-ray (EDS) analysis was then carried out to assess the elemental distribution and quantify it in particular selected regions corresponding to both hardness values. Table 1 displays the elemental mass percentages found in a selected region adjacent to the two microhardness measurements, namely, 526.13 HV and 426.12 HV. A noteworthy observation is the significantly greater carbon content in the region corresponding to the 526.13 HV measurement compared to the area linked to 426.12 HV. No other elements are detected, which supports the conclusion that the applied surface treatment for the thrust pin and insert is carburization with a minimum depth of 0.56 mm.

Table 1. Chemical composition of the selected two areas near microhardness indentation.

Chemical Element (% Mass)	526.13 HV Area	426.12 HV Area
Fe	88.67	89.26
C	5.5	5.05
Ni	3.47	3.38
Cr	1.42	1.45
Si	0.93	0.86

4.2. The Thrust Insert: AISI 9310

4.2.1. Chemical Composition

Upon comparing the acquired chemical composition with the criteria set forth by the American Iron and Steel Institute (AISI) standards, the steel grade of the thrust insert was determined to be AISI 9310. This determination was made by scrutinizing the composition of different elements found in the steel samples, beginning with the carbon content and, subsequently, concentrating on the presence of nickel and chromium in the alloyed steel (Table 2).

Table 2. Comparison of chemical composition of AISI 9310 and the insert.

Steel	Content of Elements [Mass %]			
	C	Ni	Cr	Mo
Insert	0.1	3.15	1.29	0.063
AISI 9310	0.08–0.13	3.00–3.50	1.00–1.40	0.08–0.15

AISI 9310 is categorized as a low alloy steel, containing nickel, chromium, and molybdenum. Its density is 7.85 g/cm^3 and has a melting point of 1450–1500 °C; it has good thermal and electrical conductivity, and a coefficient of thermal expansion similar to other steel alloys. The measured hardness value for the thrust insert was determined to be 355.23 HV (equivalent to 36 HRc). The following table presents the mechanical properties of AISI 9310 (Table 3).

Table 3. Mechanical properties of AISI 9310 [36].

Variable	Yield Strength R0.2	Tensile Strength Rm	Elongation at Fracture A%	Elastic Modulus E	Rockwell Hardness
Value	900 MPa	1068 MPa	15.50%	200 GPa	36

4.2.2. Optical Microstructure

The microstructure of AISI 9310 steel was tempered to achieve a medium level of hardness, resulting in a microstructure predominantly composed of tempered martensite. This observation was made using an optical microscope at magnifications of 1000× and 1500×, as shown in Figure 13.

Tempered martensite is a microstructure that emerges when martensitic steel is subjected to a temperature that initiates decomposition and the development of a mixed structure. This typically involves a blend of ferrite (a softer and more ductile phase) and cementite (a harder and more brittle phase), or, occasionally, a bainitic structure. Under microscopic examination, tempered martensite presents itself as delicate, needle-like structures evenly distributed throughout the matrix. The darker regions within the matrix signify the presence of carbides that have formed as a result of the tempering process.

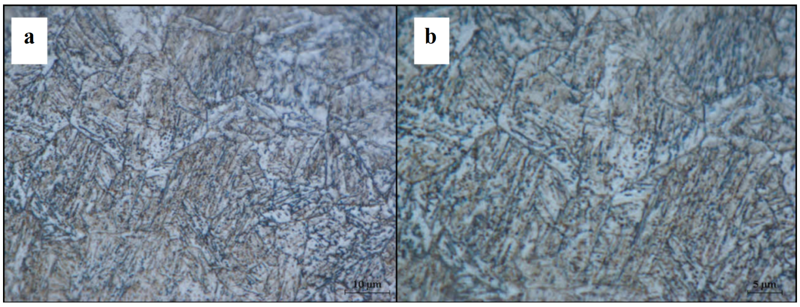

Figure 13. Optical micrographs showing microstructure of AISI 9310 at a magnification of (**a**) 1000× at a scale of 10 µm and (**b**) 1500× at a scale of 5 µm.

4.2.3. Wear Resistance

The tribological properties of AISI 9310 are crucial in determining its performance and reliability. The experiments conducted using a tribometer offer significant information about the friction and wear characteristics of AISI 9310 under different loading conditions.

Friction Force

Friction force data were captured over time for various applied loads, spanning from 4 N to 12 N, as illustrated in Figure 14. The initial transitional phase in the test, characterized by an upward trend in friction force across all applied loads, can be attributed to the initial resistance to motion at the beginning of the test. Following a sufficient period, the curves begin to reach a state of stability.

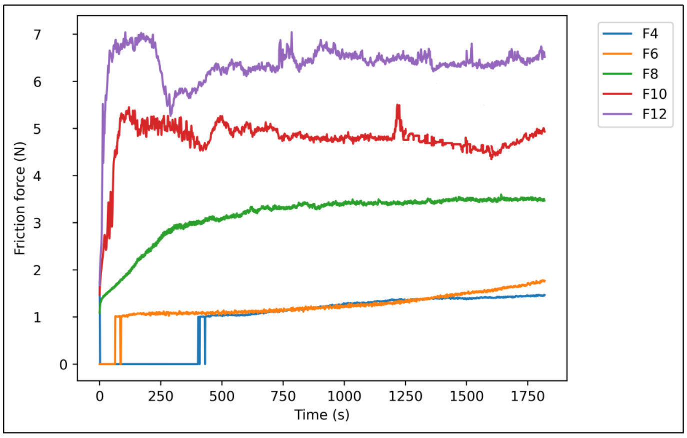

Figure 14. Variation of friction force as a function of time for different applied loads.

This suggests that the contact surfaces reached a stable condition where the friction force remained relatively consistent. It indicates that the steel's reaction to the applied load had attained an equilibrium state. It is worth noting that the findings reveal that applying a load of 4 N had a comparable impact on the friction force as applying a 6 N load. However, a rise in the friction force was observed for higher loads of 8 N, 10 N, and 12 N. This implies that the frictional characteristics of AISI 9310 steel become more prominent and reactive as the applied load reaches 8 N.

Frictio Coefficient

The friction coefficient serves as a measure of the resistance encountered during the sliding motion between two contacting surfaces. It is determined by dividing the recorded friction force by the applied load at each data point. Figure 15 illustrates the variation in the average friction coefficient value after a sliding distance of 200 m, corresponding to different applied loads. As the applied load escalates, the friction coefficient exhibits a concurrent increase, signifying that the surfaces in contact (specifically, the ball on the AISI 9310 sample) encounter heightened resistance to motion. This rise in the friction coefficient is attributable to the augmentation of contact pressure between the surfaces with increasing load, resulting in a stronger interaction and a higher friction coefficient.

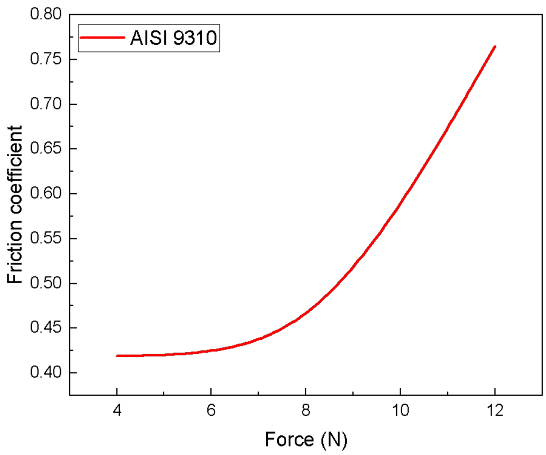

Figure 15. Variation of friction coefficient as a function of load applied for AISI 9310 steel.

Profilometer Wear Analysis

Results derived from profilometer wear analysis revealed the wear characteristics of AISI 9310 steel under varying applied forces; while the initial wear depth and area graphs demonstrated consistent variations, the primary focus turned towards the wear coefficient graph resulting from these measurements. The wear coefficient displayed minimal escalation for smaller loads, underscoring the material's impressive resistance to wear under such conditions. Nevertheless, a substantial increase in the wear coefficient became evident at the applied force of 12 N, reaching its peak at 42.709×10^{-5} $mm^3/N.m$, as showcased in Figure 16, where its resistance to wear diminishes due to increased frictional forces and abrasive actions, leading to the generation of wear particles in the wear groove, making the resistance lower, i.e., higher wear coefficient.

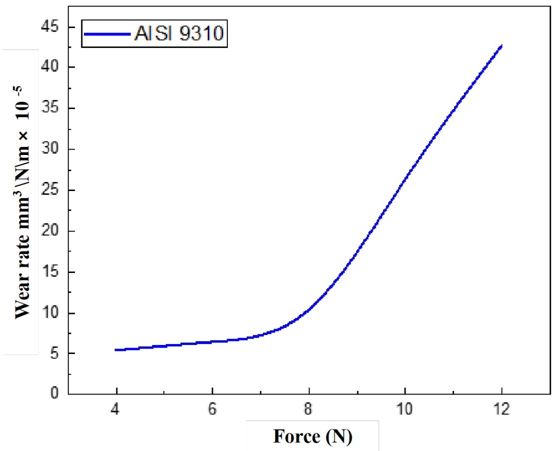

Figure 16. Variation of wear coefficient of AISI 9310 according to different applied loads.

SEM Wear Characterization

A comprehensive wear groove micrograph was also captured for AISI 9310 steel to evaluate the extent of surface damage. It is important to emphasize that an SEM was exclusively utilized for the 12 N force test. This particular test was selected because it exhibited a notable increase in wear coefficient compared to other force levels, rendering it a crucial point for analysis.

The same technique, involving the use of an Everhart Thornley Detector (ETD) in secondary electron (SE) mode, was applied to acquire a three-dimensional perspective. The working distance for this specific micrograph was set at 34.6 mm. Upon scrutinizing the micrograph, it becomes evident that AISI 9310 steel had undergone significant wear. The surface damage was distributed throughout the wear groove, displaying a variety of distinct types of damage.

Figure 17 displays an SEM micrograph that illustrates the worn surface of AISI 9310 steel, which was subjected to a coefficient of friction of 0.53. The surface exhibits a combination of both smooth and rough regions. The presence of these rough areas is significant, as they imply substantial wear. These rough patches signify locations where there has been considerable material removal, likely attributable to localized deformation and damage resulting from the interaction between the sliding surfaces.

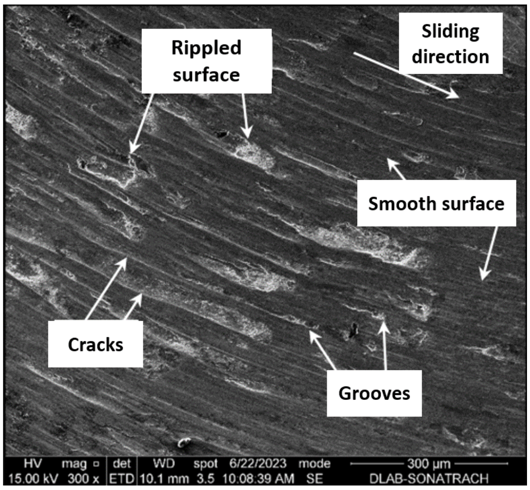

Figure 17. SEM micrograph of worn morphology for AISI 9310 steel wear groove with different damages.

The presence of debris is a consequence of a micro-cutting mechanism that occurs between the contacting surfaces during the sliding process, where the surfaces undergo shear forces and localized stresses. As reported by Li and Tandon (2000) [37], these forces and stresses can induce a micro-cutting action, causing small material fragments to be sheared off from the surface, detached, and then transferred onto the surface. These fragments act as abrasive particles within the sliding surfaces, further intensifying the wear process. In addition to the predominant wear observed in the form of rough patches, the micro-cutting mechanism also plays a role in the overall wear process, potentially leading to material removal and surface damage. The process of micro-cutting was investigated and observed in a study by Lim and Brunton (1985) [38], where a pin-on-disc wear rig was built specifically to function within a scanning electron microscope (SEM), enabling direct observations of the wear process. This setup unveiled two fundamental mechanisms: one involving cutting, and the other involving the accumulation of wedges with debris resembling flakes. It is worth noting that the presence of oxides, in the form of debris (Figure 18), could have implications for tribo-corrosion, a phenomenon arising from the interaction of mechanical wear and oxidation when a material experiences both sliding contact and exposure to an oxidizing environment.

The presence of oxides implies the possibility of concurrent wear and oxidation during the sliding process. When material surfaces make contact with each other, frictional forces generate heat, potentially causing localized areas to reach higher temperatures. These elevated temperatures, coupled with the presence of an oxidizing environment (such as humidity, in this case), can result in the formation of oxides on the material's surface. The presence of these oxides can worsen the wear process, as they act as abrasive particles, intensifying material removal and surface damage.

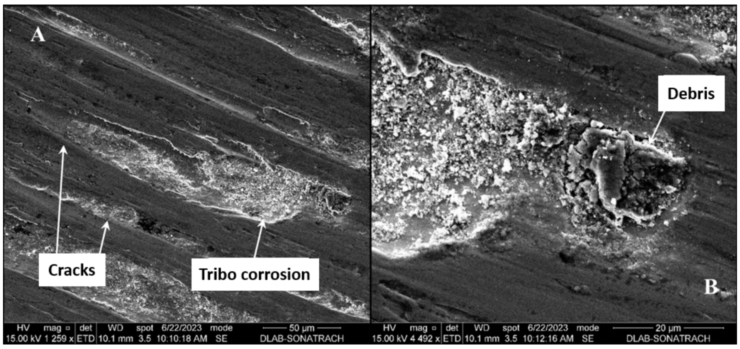

Figure 18. SEM micrographs of worn morphology for AISI 9310 steel with a magnification of (**A**) 1259× and (**B**) 4492×.

Furthermore, the oxides might also establish localized electrochemical cells, which can accelerate oxidation in those specific areas. The occurrence of tribo-corrosion in AISI 9310 steel holds significance for the material's durability and performance in situations where both sliding and oxidizing conditions are encountered. The transformation of wear debris into iron oxides under high load and sliding speeds, as described by Stachowiak and Batchelor (2005) [39], supports the observed oxidative wear in AISI 9310, emphasizing the role of temperature and environmental conditions in this process. To gain a better understanding of the composition of debris and distribution on the material surface, a more detailed investigation and analysis of these oxides is warranted. An EDS analysis was conducted on a different surface area with a higher prevalence of oxides. Findings are presented in Table 4. For the analysis, five spots were selected, representing various regions of the micrograph, spanning from the lightest to the darkest areas. Spots 1 and 2 were positioned in the darkest and lightest regions, respectively. The analysis unveiled that the first spot contained mineral salts, with sodium (Na) being the dominant element at a concentration of 1.45%.

Table 4. Spots with different mass percentages of chemical elements.

		Spot Number				
		1	**2**	**3**	**4**	**5**
Chemical elements [mass %]	**Fe**	48.39	80.52	55.55	46	61.37
	C	30.73	14.48	13.4	15.87	18.39
	Cr	1.4	1.24	1.09	0.89	1.27
	Ni	2.31	2.97	2.2	2.34	2.72
	O	7.22	/	27.04	33.45	15.59
	N	4	/	/	/	/
	Cl	0.76	/	/	0.8	/
	K	0.86	/	/	/	/
	Ca	1.3	/	/	/	/
	Si	0.76	0.78	0.72	0.65	0.66
	Na	1.45	/	/	/	/
	S	0.82	/	/	/	/

The existence of these salts could be attributed to moisture accumulation. Conversely, the second spot, situated in the lightest region, suggests the absence of oxygen indicating no oxidation. The remaining three spots (3, 4, and 5), which were selected from grayish regions featuring visible debris, all displayed the presence of oxygen at varying percentages. This serves to confirm the existence of oxides within the debris.

Spot number 4 notably exhibited the highest oxygen percentage among the three spots, indicating a more concentrated presence of oxides in that particular area. This discovery lends support to the hypothesis that this specific spot or region is closely associated with the presence of oxides. The identification of these oxides within the debris strongly suggests the occurrence of tribo-corrosion, a phenomenon frequently observed in low-alloy steel, as it was investigated before by Lee et al. (2015) [40].

4.3. The Thrust Pin: AISI 9314

4.3.1. Chemical Composition

The thrust insert was determined to be made of AISI 9314 steel, a nickel-chromium-molybdenum case-hardening alloy renowned for its exceptional attributes of high strength, toughness, and hardenability. This steel is widely employed in applications necessitating robust performance, such as gears, crankshafts, and heavy-duty machinery components (Table 5).

Table 5. Comparison of chemical composition of AISI 9314 and the pin.

Steel	**Content of Elements [Mass %]**			
	C	**Ni**	**Cr**	**Mo**
Pin	0.13	3.35	1.28	0.064
AISI 9314	0.11–0.17	3.00–3.50	1.00–1.40	0.08–0.15

The hardness value determined for AISI 9314 steel was recorded at 400.15 HV (equivalent to 41 HRc). The following table presents the mechanical properties of AISI 9314 (Table 6).

Table 6. Mechanical properties of AISI 9314 [41].

Variable	**Yield Strength R0.2**	**Tensile Strength Rm**	**Elongation at Fracture A%**	**Elastic Modulus E**	**Rockwell Hardness**
Value	1034 MPa	1158 MPa	15%	190–210 GPa	41

4.3.2. Optical Microstructure

AISI 9314 steel, with a hardness of 41 HRC, exhibits a microstructure characterized by tempered martensite, much like AISI 9310. This particular microstructure can be observed using an optical microscope at magnifications of 1000× and 1500×, as depicted in Figure 19.

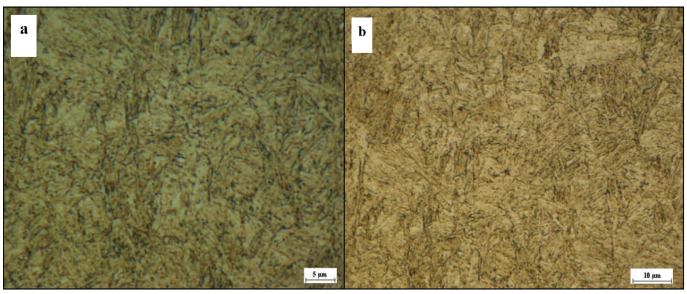

Figure 19. Optical micrographs showing microstructure of AISI 9314 at a magnification of (**a**) 1000× at a scale of 5 µm and (**b**) 1500× at a scale of 10 µm.

4.3.3. Wear Resistance

Understanding the tribological behavior of AISI 9314 is of utmost importance to ensure efficient and dependable performance in engineering applications. This widely employed steel alloy possesses outstanding mechanical properties.

The primary goal of this study is to delve into the friction and wear characteristics of AISI 9314 steel and to analyze how the friction coefficient and friction force vary under diverse applied loads.

Friction Force

Friction force measurements were logged over time for each load in the range of 4 N to 12 N, as shown in Figure 20. Much like the friction force variation observed in the case of AISI 9310, an initial transitional phase in the test was noted, marked by an increase in friction force for all applied loads. Subsequently, as the applied load increased, the duration of this transitional phase also extended, eventually leading to the stabilization of the curves.

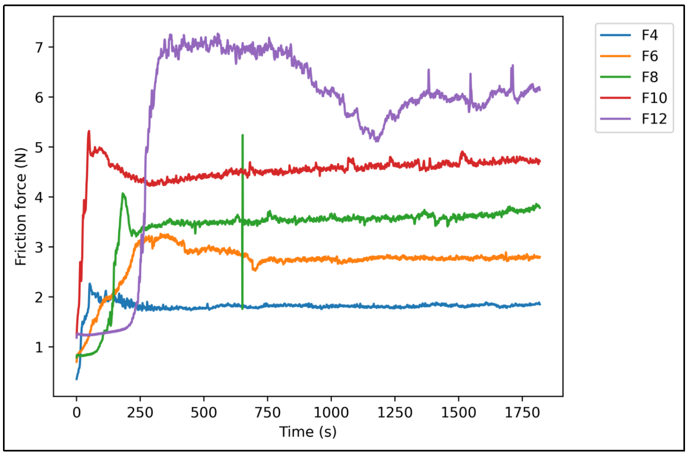

Figure 20. Variation of friction force as a function of time for different loads applied.

Friction Coefficient

Derived from the tribometer testing carried out on AISI 9314 using various loads (4 N, 6 N, 8 N, 10 N, and 12 N), Figure 21 illustrates the average friction coefficient values obtained after sliding a distance of 200 m, corresponding to the applied loads.

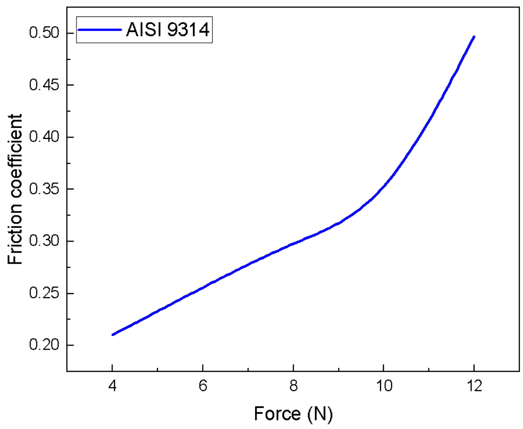

Figure 21. Variation of friction coefficient as a function of load applied for AISI 9314 steel.

The graph clearly reveals a pattern of rising friction coefficients as the load increases, particularly beyond 10 N. This trend suggests that, as the load escalates, there may be an enlargement of the contact area between the AISI 9314 steel material and the mating surface. This expanded contact area can lead to heightened adhesion and frictional forces between the surfaces, ultimately resulting in an elevated friction coefficient.

Profilometer Wear Analysis

Following profilometer measurements on the surface, the system processes the data to ascertain parameters such as wear area, wear depth, and, notably, wear coefficient. Figure 22 displays the variation in wear coefficient as a function of applied load after a sliding distance of 200 m.

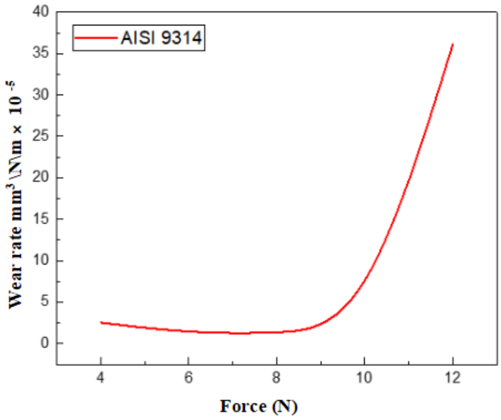

Figure 22. Variation of wear coefficient of AISI 9314 according to different applied load.

For smaller loads, there is no noticeable upward trend in the wear coefficient, signifying the material's robust wear resistance against lighter forces. However, when the applied load reaches 12 N, the wear coefficient escalates to 36.121 $\times$ 10^{-5} $mm^3/N.m$.

SEM Wear Characterization

SEM analysis was utilized to investigate the worn surface of AISI 9314 steel, aiming to understand the wear mechanisms. A complete wear groove was imaged to provide an overall assessment of the surface damage, with the analysis conducted from a working distance of 26.3 mm. The micrograph clearly indicates that the material experienced significant wear, with surface damage distributed throughout the wear groove, showcasing various types of damage. Further examination and description of these different types of damage can offer a more comprehensive understanding. Figure 23 displays the worn morphology of AISI 9314 steel as observed with an SEM, which resulted in a friction coefficient of f = 0.528. The material's surface exhibits a combination of smooth and rough areas. The rough patches on the surface are particularly intriguing, as they signify predominant wear. Similarly described by Prathipati et al. (2020) [42], within these rough patches, a rippled surface is discernible, indicating significant material removal.

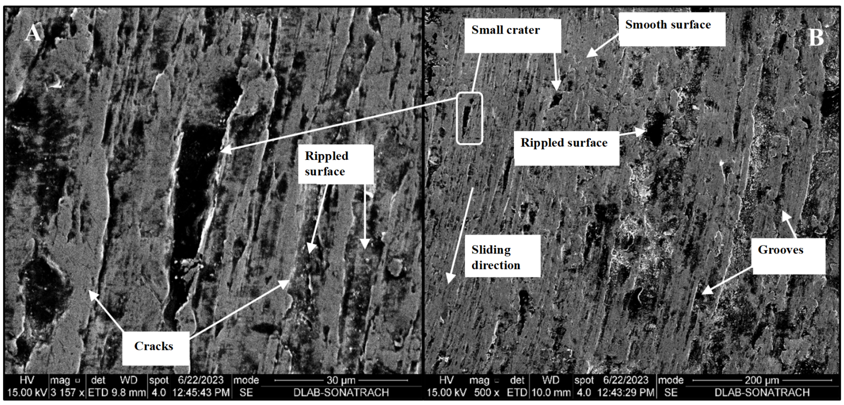

Figure 23. SEM micrograph of worn morphology of AISI 9314 with different magnifications, and damages (**A**) 3157×, and (**B**) 500×.

These ripples likely result from the interaction between the sliding surfaces, leading to localized deformation and damage that can be be attributed to the presence of adhesive wear formerly occurring when the material sticks and then tears away as the surfaces slide past each other. These findings match those by Karaoğlu (2002) [43], who evaluated the wear behavior of plasma-nitrided AISI 5140 low-alloy steel using SEM revealing extensive wear by adhesion due to local fusion. Furthermore, Figure 23A illustrates the presence of a crater on the material surface. This crater formed as a consequence of the sliding action and represents a localized area where material has been removed.

Notably, there is no debris evident within the crater, suggesting that any loose particles or wear debris generated during the sliding process have been displaced from the area by subsequent cycles. The shape and characteristics of the crater offer significant findings of the wear mechanism that occurred. The presence of cracks in the proximity of the crater suggests that surface dislocations and damage occurred during the sliding process. These cracks may have originated and propagated due to the stress and strain imposed on the material as a consequence of sliding contact, potentially marking the initiation of fatigue wear. Li and Tandon (2000) [37] noted the presence of cracks and microvoids in the Fe-rich sublayers of similar materials, which could form during the compaction of mixed material layers (MML) or as a result of deformation from continued sliding wear. This observation is crucial, as it indicates that the microvoids and cracks observed near the crater in AISI 9314 might also be attributable to the initiation of fatigue, exacerbated by the repetitive stress and microstructural changes inherent in the sliding process.

In summary, Figure 23A,B depict the worn surface of AISI 9314 steel. The presence of both smooth and rough patches, coupled with a rippled surface and a crater, signifies substantial wear and localized material removal. These observations provide clues regarding the wear mechanisms involved, which encompass micro-cutting, surface dislocations, damage, and the potential for crack formation.

4.4. Summary of Findings and Implications

In this paper, we aimed to provide a comprehensive analysis of the wear resistance of thrust pins and inserts used in high-speed drilling motors, focusing on the materials AISI 9314 and AISI 9310. The AISI 9314 thrust pin demonstrated superior wear resistance, as expected, likely due to its higher hardness and tempered martensite microstructure, while the AISI 9310 insert exhibited less wear resistance, potentially due to its lower hardness level, which may not suffice under the demanding conditions of high-speed drilling.

The differential performance observed prompts a discussion on the practical implications for drilling operations, where enhanced wear resistance translates to improved efficiency and safety. This study's findings suggest a critical reevaluation of material selection, especially for the AISI 9310 insert, to ensure the optimal performance and longevity of drilling components.

Future research might explore alternative materials or surface treatments to enhance the wear resistance of the AISI 9310 insert. Additionally, further investigation into the microstructural characteristics that contribute to superior wear resistance could provide valuable insights for material engineering and selection in high-speed drilling and similar applications; while this study provides a foundational understanding of material wear characteristics, ongoing research is essential to develop more resilient and efficient materials for demanding industrial applications.

5. Conclusions

This research provides an in-depth analysis of the wear resistance of thrust pins and inserts, specifically AISI 9314 and AISI 9310, used in high-speed drilling motors. The study reveals that the AISI 9314 thrust pin exhibits superior wear resistance due to its higher hardness and tempered martensite microstructure. Conversely, the AISI 9310 insert shows less wear resistance than expected, likely due to its lower hardness, indicating that it may not be suitable for the demanding conditions of high-speed drilling. The findings are significant for materials engineering in the oil and gas industry, particularly in optimizing drilling motor components. The superior performance of the AISI 9314 thrust pin over the AISI 9310 insert highlights the need for further improvements in materials or treatment processes, especially for the insert. Such optimization could enhance drilling motor performance and contribute to reducing CO_2 emissions, aligning with sustainable energy practices.

Moreover, this research opens avenues for future studies to investigate the effects of different surface treatments, such as carburizing, on wear resistance. This could extend the lifespan of drilling motors and improve their performance. The study serves as a valuable resource for researchers and engineers focusing on the wear performance of drilling components and the potential of alternative materials or treatments. In conclusion, the research has broad implications for the oil and gas industry. Enhancing the wear resistance of key components like thrust pins and inserts can lead to more efficient drilling operations, reduced downtime, and increased productivity. These improvements can result in significant economic benefits, such as lower maintenance costs and longer component lifespans, while also supporting environmental sustainability through reduced CO_2 emissions.

To enhance the scope of this study, several perspectives should be taken into account:

- Long-term wear testing under realistic operating conditions can provide insights into the actual lifetime of these components.
- Developing wear models and simulations can predict the lifetime based on wear mechanisms, drilling parameters, and material properties.
- Advanced material characterization techniques, such as in situ microscopy and surface analysis, can identify critical wear parameters and failure modes.
- Further research on potential surface treatments to enhance wear resistance and operational lifespan of drilling components.
- Continuously exploring and developing novel steel alloys with enhanced wear resistance properties can improve component lifetimes.

Author Contributions: Methodology, A.B.; Investigation, A.B., H.K. and S.B.; Writing—original draft, A.B., A.L., H.K. and S.B.; Writing—review & editing, A.B., O.S.T., A.L. and K.A.; Supervision, O.S.T. and K.A. All authors have read and agreed to the published version of the manuscript.

Funding: This research received no external funding.

Institutional Review Board Statement: Not applicable.

Informed Consent Statement: Not applicable.

Data Availability Statement: The original contributions presented in the study are included in the article, further inquiries can be directed to the corresponding authors.

Acknowledgments: Declaration of AI and AI-assisted technologies in the writing process: during the preparation of this work the authors used ChatGPT in order to improve readability and language. After using this tool/service, the authors reviewed and edited the content as needed and takes full responsibility for the content of the publication.

Conflicts of Interest: The authors declare no conflicts of interest.

References

1. Ashrafizadeh, H.; McDonald, A.; Mertiny, P. Erosive and abrasive wear resistance of polyurethane liners. In *Aspects of Polyurethanes*; IntechOpen: London, UK, 2017. [CrossRef]
2. Tremmel, S.; Marian, M. Current Trends and Applications of Machine Learning in Tribology—A review. *Lubricants* **2021**, *9*, 86. [CrossRef]
3. BC Oil and Gas Commission. *Oil and Gas Wells: Drilling Activity*; Technical Report; BC Energy Regulator: Fort St John, BC, Canada, 2019.
4. Drilling Industry Glossary | Support and Resources. (n.d.). Available online: https://www.pvisoftware.com/drilling-industry-glossary.html (accessed on 1 July 2023).
5. Al-Safran, E.; Nguyen, V.T.; Nguyen, T. Theoretical modeling of Positive Displacement Motors performance. *J. Pet. Sci. Eng.* **2018**, *166*, 188–197. [CrossRef]

6. Picksak, A.; John, W.; Regener, T.; Reich, M. Competitive Performance Drilling with High-Speed Downhole Motors in Hard and Abrasive Formations. In Proceedings of the IADC/SPE Drilling Conference, New Orleans, LA, USA, 23–25 February 2000. [CrossRef]
7. Neelgund, R.; Smith, D.L.; Blackman, W.; Li, F. Drilling Dynamics Measurements on Positive Displacement Motors pdm Enhance Performances and Reliability. In Proceedings of the International Petroleum Technology Conference, Beijing, China, 26–28 March 2019. [CrossRef]
8. Halwani, M.; Swart, D.; Muthusamy, R.; Almaskari, F.; Zweiri, Y.; Ayyad, A. Neuromorphic vision based control for the precise positioning of robotic drilling systems. *Robot. Comput.-Integr. Manuf.* **2023**, *79*, 102419. [CrossRef]
9. Hoteit, H.; Albattat, R. A semi-analytical approach to model drilling fluid leakage into fractured formation. *Rheol. Acta* **2021**, *60*, 353–370. [CrossRef]
10. Von Gynz-rekowski, G.H.; Bolejack, D.E.; Herben, W.C. Mud Motor Bearing Assembly and Method. U.S. Patent No. 9,267,539, 23 February 2016. Available online: https://www.freepatentsonline.com/9267539.html (accessed on 15 July 2023).
11. Drilling Motor Handbook, Volume 2. Scientific. 2018. Available online: https://www.scribd.com/document/501657996/2018 (accessed on 15 July 2023).
12. Drilling Mud Motor Components Operations. Drilling Manual. 2017. Available online: https://www.drillingmanual.com/downhole-drilling-mud-motors-components-diagram/ (accessed on 20 July 2023).
13. Kecibas, G.; Besirova, C.; Chehrehzad, M.R.; Burun, G.; Pehlivan, T.; Uresin, U.; Emekli, E.; Lazoglu, I.; Bilgili, D. Tool flank wear prediction using high-frequency machine data from industrial edge device. *Procedia CIRP* **2023**, *118*, 483–488. [CrossRef]
14. Holmberg, K.; Kivikytö-Reponen, P.; Härkisaari, P.; Valtonen, K.; Erdemir, A. Global energy consumption due to friction and wear in the mining industry. *Tribol. Int.* **2017**, *115*, 116–139. [CrossRef]
15. Holmberg, K.; Erdemir, A. The impact of tribology on energy use and CO_2 emission globally and in combustion engine and electric cars. *Tribol. Int.* **2019**, *135*, 389–396. [CrossRef]
16. Wheeler, D. Applications of diamond to improve tribological performance in the oil and gas industry. *Lubricants* **2018**, *6*, 84. [CrossRef]
17. Sexton, T.; Cooley, C. Polycrystalline diamond thrust bearings for down-hole oil and gas drilling tools. *Wear* **2009**, *267*, 1041–1045. [CrossRef]
18. Vakis, A.I.; Yastrebov, V.; Scheibert, J.; Nicola, L.; Dini, D.; Minfray, C.; Almqvist, A.; Paggi, M.; Lee, S.; Limbert, G.; et al. Modeling and simulation in tribology across scales: An overview. *Tribol. Int.* **2018**, *125*, 169–199. [CrossRef]
19. Dzaky, D.M.; Aziz, A.; Saefulloh, I.; Susilo, S.; Hasanah, I.U. Rancang Bangun Chasis Pin Holder Pada Tribometer Pin On Disc Berbasis Modifikasi Pada Mesin Bubut Konvensional. *JPTM J. Pendidik. Tek. Mesin* **2021**, *8*, 173–179. [CrossRef]
20. Böttcher, R.; Winkler, H.; Dienwiebel, M.; Scherge, M. Tribology of Wire Arc Spray Coatings under the Influence of Regenerative Fuels. *Lubricants* **2018**, *6*, 60. [CrossRef]
21. Ahmer, S.M.H.; Khan, N.; Shah, S.I.A.; Jan, L.S. Experimental results of the tribology of aluminum in the presence of polytron additive. In *Friction, Lubrication and Wear*; IntechOpen: London, UK, 2019. [CrossRef]
22. Viña, J.; García, M.C.; Castrillo, M.Á.B.; Viña, I.; Argüelles, A. Wear behavior of a glass Fiber-Reinforced PEI composite. *J. Thermoplast. Compos. Mater.* **2008**, *21*, 279–286. [CrossRef]
23. Bill, R.C. Fretting of AISI 9310 steel and selected Fretting-Resistant surface treatments. *Tribol. Trans.* **1978**, *21*, 236–242. [CrossRef]
24. Hartley, N.E.W.; Hirvonen, J. Wear testing under high load conditions. *Nucl. Instruments Methods Phys. Res.* **1983**, *209–210*, 933–940. [CrossRef]
25. Yan, H.; Wei, P.; Su, L.; Liu, H.; Wang, D.; Zhang, X.; Deng, G. Rolling-sliding contact fatigue failure and associated evolutions of microstructure, crystallographic orientation and residual stress of AISI 9310 gear steel. *Int. J. Fatigue* **2023**, *170*, 107511. [CrossRef]
26. Ganechari, S.M.; Kabadi, V.R.; Kori, S. Study of Surface Roughness and Hardness of Low Carbon Nickel-Chromium Based Alloy Steels under High Temperature (AISI sae8630, 3140 and 9310). In Proceedings of the ICWET'11 International Conference and Workshop on Emerging Trends in Technology, Mumbai, Maharashtra, India, 25–26 February 2011. [CrossRef]
27. Li, X.; Zhou, L.; Zhao, T.; Pan, X.; Liu, P. Research on Wear Resistance of AISI 9310 Steel with Micro-Laser Shock Peening. *Metals* **2022**, *12*, 2157. [CrossRef]
28. Hegadekatte, V.; Kurzenhäuser, S.; Huber, N.; Kraft, O. A predictive modeling scheme for wear in tribometers. *Tribol. Int.* **2008**, *41*, 1020–1031. [CrossRef]
29. Suresh, R.; Kumar, M.; Basavarajappa, S.; Kiran, T.; Yeole, M.; Katare, N. Numerical Simulation Experimental study of wear depth and Contact pressure distribution Of Aluminum MMC Pin on Disc Tribometer. *Mater. Today Proc.* **2017**, *4*, 11218–11228. [CrossRef]
30. *ASTM E415*; Standard Test Method for Analysis of Carbon and Low-Alloy Steel by Spark Atomic Emission Spectrometry. ASTM International: West Conshohocken, PA, USA, 2015.
31. *ASTM E407*; Standard Practice for Microetching Metals and Alloys. ASTM International: West Conshohocken, PA, USA, 2007.
32. *ASTM E18*; Standard Test Methods for Rockwell Hardness of Metallic Materials. ASTM International: West Conshohocken, PA, USA, 2020.
33. *ASTM E384*; Standard Test Method for Microindentation Hardness of Materials. ASTM International: West Conshohocken, PA, USA, 2022.

34. *ISO 7148*; Plain Bearings—Testing of the Tribological Behavior of Bearing Materials. International Organization for Standards: Geneva, Switzerland, 2012.
35. *ASTM E1508*; Standard Guide for Quantitative Analysis by Energy-Dispersive Spectroscopy. ASTM International: West Conshohocken, PA, USA, 2019.
36. Karia, P. SAE—AISI 9310 Alloy Steel—Properties, Composition and Uses. The Piping Mart Blog. Available online: https://tinyurl.com/msmhv7b7 (accessed on 5 May 2023).
37. Li, X.; Tandon, K.N. Microstructural characterization of mechanically mixed layer and wear debris in sliding wear of an Al alloy and an Al based composite. *Wear* **2000**, *245*, 148–161. [CrossRef]
38. Lim, S.; Brunton, J.H. A dynamic wear rig for the scanning electron microscope. *Wear* **1985**, *101*, 81–91. [CrossRef]
39. Stachowiak, G.; Batchelor, A.W. *13—Corrosive and Oxidative Wear, Engineering Tribology*, 3rd ed.; Butterworth-Heinemann: Oxford, UK, 2005; pp. 573–593. ISBN 9780750678360.
40. Lee, T.; Mathew, E.V.; Rajaraman, S.; Manivasagam, G.; Singh, A.K.; Lee, C.S. Tribological and corrosion behaviors of warm- and hot-rolled Ti-13Nb-13Zr alloys in simulated body fluid conditions. *Int. J. Nanomed.* **2015**, *2015*, 207. [CrossRef]
41. Steel Grades. (n.d.). Datasheet for Steel Grades Carbon Steel AISI E9314. Available online: https://tinyurl.com/4xffb4f2 (accessed on 20 July 2023).
42. Prathipati, R.; Dora, S.P.; Chanamala, R. Wear behavior of wire electric discharge machined surface of 316L stainless steel. *SN Appl. Sci.* **2020**, *2*, 412. [CrossRef]
43. Karaoğlu, S. Structural characterization and wear behavior of plasma-nitrided AISI 5140 low-alloy steel. *Mater. Charact.* **2002**, *49*, 349–357. [CrossRef]